European Journal of Engineering and Applied Sciences

ISSN: 2651-3412 (Print) & 2667-8454 (Online)
Journal homepage: http://dergipark.gov.tr/EJEAS
Published by Çorlu Faculty of Engineering, Tekirdağ Namık Kemal University

European J. Eng. App. Sci. 7(2), 150-158, 2024

Research Article

A Water Absorption Chamber Design for Cable Capacitance Measurement Tests

Ercan Ulutay [1,a], Metin Yurtsever [1,b], Avşin Öztaş[1,c], Uğur Akyol[2,d], Reşat Mutlu[3,e,*],

[1] Ünika Üniversal Kablo Sanayi ve Tic. A.Ş.. Veliköy Sanayi Bölgesi Çerkezköy - Tekirdağ , Turkey, 59500
[2]Mechanical Engineering, Corlu Faculty of Engineering, Tekirdağ Namık Kemal University, Tekirdağ , Turkey, 59860
[3]Electrical-Electronics Engineering, Corlu Faculty of Engineering, Tekirdağ Namık Kemal University, Tekirdağ , Turkey, 59860

[a]ercan.ulutay@unika.com.tr, [b]metin.yurtsever@unika.com.tr, [c]avsin.oztas@unika.com.tr, [d]uakyol@nku.edu.tr, [c]rmutlu@nku.edu.tr

Received: 08.12.2024 Accepted: 27.12.2024 DOI: 10.55581/ejeas.1598086

Abstract: XLPO cables used in ships should be tested for water absorption. Test standards require the cables be submerged in a water absorption chamber and kept at 75 ^{0}C for 14 days. Once every 7 days, the cables within the chamber are tested by applying high voltage, and their capacitance, dissipation factor, stability factor, and relative Permittivity are measured. In this study, a water absorption chamber used in the experiments is designed using fiberglass material and controlled with an ENDA ET 4420 temperature controller. It is experimentally shown that the water absorption chamber performs well.

Keywords: *Power Cables, Water Absorption Test, Cable Tests, Thermal Design, Heater Design.*

Kablo Kapasitans Ölçüm Testleri için Su Emme Odası Tasarımı

Öz. Gemilerde kullanılan XLPO kablolar su emme açısından test edilmelidir. Test standartları, kabloların su emme odasına batırılıp 75 ^{0}C'de 14 gün saklanmasını gerektirmektedir. Her 7 günde bir, oda içerisindeki kablolar yüksek gerilim uygulanarak test edilerek kapasite, kayıp faktörü, stabilite faktörü ve bağıl geçirgenlik ölçümleri yapılır. Bu çalışmada deneylerde kullanılan bir su emme odası fiberglas malzeme kullanılarak tasarlanmış ve bir ENDA ET 4420 sıcaklık kontrolörü kullanarak kontrol edilmiştir. Deneysel olarak su emme odasının iyi başarımla çalıştığı gösterilmiştir.

Anahtar Kelimeler: *Güç Kabloları, Su Emme Testi, Kablo Testleri, Termal Tasarım, Isıtıcı Tasarımı*

.1. Introduction

Cables, which are an important part of electrical systems, should be tested according to standards [1-4]. Marine cables are an important cable type, and their market share is ever-increasing [5, 6]. Marine cables also age due to water trees occurring within [7, 8]. Marine cables are tested according to IEEE 1580-2021, NEMA WC 53, and NEMA WC 57 to make sure that they operate without failure [9-11]. The Accelerated Water Absorption test is defined in the IEEE 1580:2021 standard [9]. The electrical and mechanical tests are performed on the insulation material of the cable after removing its sheath according to Table 13 given in IEEE 1580-2021 standard. All the values measured are used to calculate the dielectric constant, capacitance increase, and stability factor and the calculated cable parameters are compared to the standard values given in Table 13 of the IEEE 1580-2021 standard [10]. After the comparison, it can be decided whether the test is successful or not. The note at the bottom of Table 13 refers to Section 6.14 of the standard NEMA WC 57 for the test procedure [11]. Information about the cables to be tested is given in the NEMA WC 57 standard, and, therein, it is stated that the test can be done in two different methods which are the electrical and gravimetric methods. The electrical method is defined in the IEEE 1580-2021 standard for testing. NEMA WC 57 standard tests and calculations direct us to the NEMA

* Corresponding author
E-mail address: rmutlu@nku.edu.tr (R. Mutlu)

WC 53 standard (Section 2.6 of NEMA WC 53) [10]. The tests specified in the IEEE 1580-2021, Table 13 Accelerated Water Absorption section of the NEMA WC 53 standard are explained and how the calculations can be made is stated. A low-voltage XLPO cable is tested using an accelerated water absorption test [12].

A water chamber should be used during the testing of marine cables according to IEEE 1580-2021. Such a water chamber must be designed to keep the water temperature at 75 ^{0}C [9, 12]. A water heater design needs a good experience [12]. The electrical heaters can be controlled using several different techniques [13-15]. In [16-20], a PLC is used for this purpose. A PID controller is preferred in [18, 19, 21]. A microcontroller is used to design an intelligent bath water heater [22]. The temperature of a water heater must be sensed with an accurate temperature sensor [14, 23]. The temperature of electrical heaters can be monitored with a transmitter [24]. The effect of several parameters on a heater is studied to increase its efficiency [25]. Such a water chamber must be designed using good heat insulators and good controllers [26]. Choosing a bad material may result in a failed operation [27]. In this study, a water test absorption chamber is designed to be used in the tests. Fiberglass is used to make the chamber due to its low thermal conductivity [28]. The temperature controller shown to perform well in the polymerization process is used to control its water temperature [29, 30]. The heat transfer model of the chamber is also made. The performance of the chamber is tested experimentally.

This paper is ordered as follows. In the second section, the water absorption bath mechanical system is introduced. In the third section, the water absorption bath electrical system is briefly described. In the fourth section, the heat transfer model of the system is given. In the fifth section, the simulation results are given. In the sixth section, the experimental results are given. The study is finished with the conclusion section.

2. Water Absorption Bath Mechanical System

A sketch of the water absorption test chamber can be seen in Figure 2. It is made of a box, a lid, and an internal grid. All the parts of the box are fiberglass which is chosen due to its low thermal conductivity and thermal endurance [28]. It can stand temperatures more than 100 ^{0}C. The lid has also two holes for guiding the cable ends in and out. The grid is used to prevent direct contact of the heater resistance to the power cable and its damage. The box has two holes. The heater resistance is placed in one of them and the thermocouple in the other. The controller circuit is placed onto the front side of the box. A photograph of the designed device is given in Figure 2.

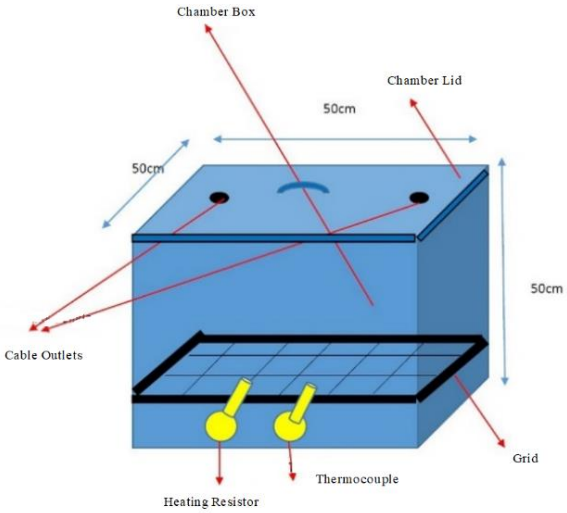

Figure 1. *A Drawing of the Water Absorption Bath.*

Figure 2. *A Photograph of the device made.*

3. Water Absorption Bath Electrical Circuit

The schematic of the Water Absorption Bath electric circuit is shown in Figure 3. It operates at 220 Volt and dissipates power up to 2000 Watt. The electrical system of the device consists of a water heater resistance, a solid-state relay ISISO ISS-100-3, a 25 A W-automat fuse, a 0/1 rotary power switch with a signal LED, a Fe-Const J Tipi thermocouple, and an ENDA ET 4420 temperature controller [29]. A 220 V 2000 W water heater resistance is used to heat water within the chamber. The components of the circuit are shown in Figure 4.

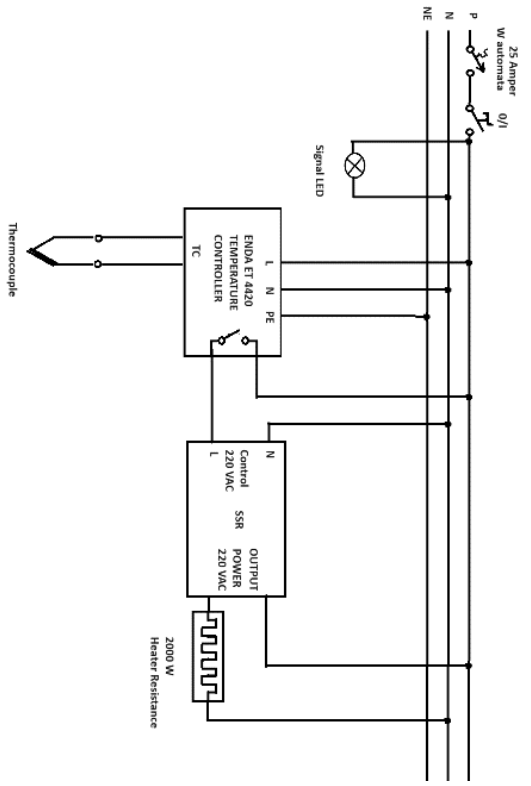

Figure 3. *Electrical Circuit of the Device.*

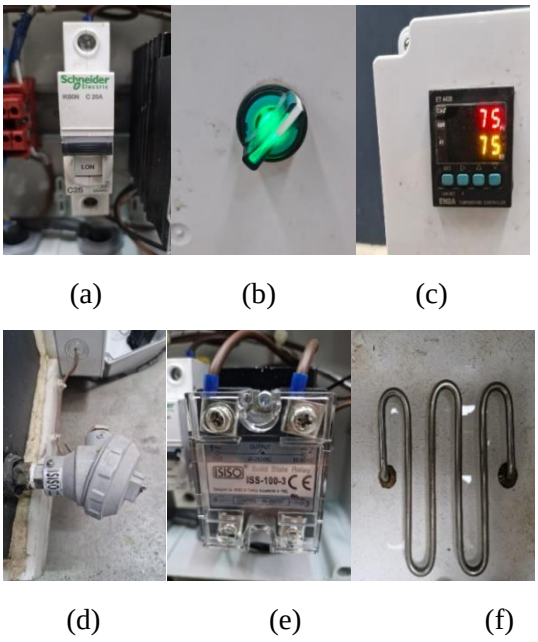

Figure 4. *The electrical components: a) a 25 A W-automat fuse (Schneider IK60N C 25A), b) a 0/1 rotary power switch with a signal LED, c) ENDA ET 4420 temperature controller, d) a Fe-Const J Tipi Thermocouple with a 25 cm long measurement probe with a diameter of 8 mm, e) the solid-state relay (SSR) ISISO ISS-100-3, and f) a 220V-2000W 18 Ohm heater resistance.*

The accuracy of a Fe-Const J Tipi thermocouple can vary depending on several factors, including the quality of the thermocouple, the measurement conditions, and the calibration. Generally, the accuracy of a Type J thermocouple is around ±2.2°C or ±0.75% of the reading, whichever is greater. Such accuracy is good enough for the test purposes.

4. On the Control of the System

A PID controller is used to control the water absorption chamber as shown in Figure 5. The PID controller parameters used in the design are given in Table 1.

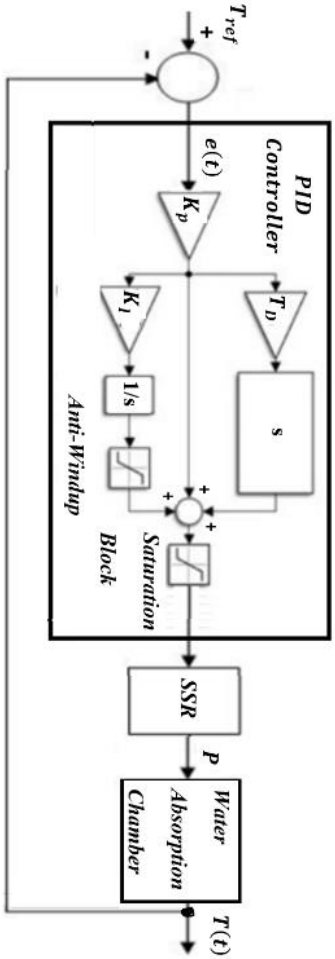

Figure 5. *PID temperature control of the water absorption chamber.*

Table 1. The PID controller parameters

The PID Parameter	Its Value
$K_p = P_b$	4
T_I	4.0 s
T_D	1.0 s
$K_I = K_p/T_I$	1 s^{-1}
$K_D = K_p T_D$	4 s

The reference water temperature is set to 75 ^{0}C degrees with ENDA ET 4420. The controller uses a hysteresis controller. When the power switch is turned on, its green LED starts illuminating and indicates that the device is energized. ENDA ET 4420 temperature controller measures the temperature using a Fe-Const J type thermocouple with a 25 cm long measurement probe with a diameter of 8 mm placed within the chamber in contact with the water. If the measured temperature is under the upper-temperature reference, the ENDA ET 4420

turns on and turns off the solid-state relay (SSR) ISISO ISS-100-3, which connects the heater resistance to the utility. The heater resistance starts heating the water and the water temperature increases. If the measured temperature reaches the upper-temperature reference, the ENDA ET 4420 turns off the solid-state relay (SSR) ISISO ISS-100-3 and the heater resistance is disconnected from the utility. The water temperature starts decreasing. When it falls to the lower-temperature reference, the ENDA ET 4420 turns on the solid-state relay (SSR) ISISO ISS-100-3 and, therefore, the heater resistance again. This operation cycle continues, and the average water temperature is kept at the set temperature of 75 ^{0}C.

The instantaneous temperature error fed to the input of the PID controller is calculated as:

$$e(t) = T(t) - T_{ref} \tag{1}$$

where $T(t)$ is the instantaneous measured water temperature and T_{ref} is the reference temperature.

The controller output PID_{out} can be expressed as:

$$PID_{out} = K_P e(t) + K_I \int_0^t e(t)dt + K_D \frac{de(t)}{dt} \tag{2}$$

Where K_P, K_I, and K_D is the proportional, the integral, and the derivative constants of the PID controller, respectively.

The controller output PID_{out}, is equal to the duty ratio of the heater power:

$$D = PID_{out} \tag{3}$$

where D is the duty ratio.

When the heater resistance is fed by the utility, the power consumed by the heater resistance is given as

$$P_{heater} = R_{AC} I_{rms}^2 \tag{4}$$

or

$$P_{heater} = V_{rms}^2 / R_{AC}(T) \tag{5}$$

where I_{rms} is the rms current of the heater resistance, V_{rms} is the rms voltage of the utility, and $R_{AC}(T)$ is the temperature dependent heater resistance.

The average power of the heater is given as

$$p = DP = R_{AC} I_{rms}^2 = D V_{rms}^2 / R_{AC}(T) \tag{6}$$

5. Heat Transfer Model of the System

In this section, a simplified thermal circuit model of the circuit is provided. The geometry of the chamber in the study consists of four vertical walls and two horizontal walls as shown in Figure 6. It is assumed that the heat transfer between the water chamber with a certain amount of water inside and a certain amount of air above the water surface and the external environment is realized by heat conduction in the solid material, while the heat transfer between the solid surfaces and the fluid interfaces is realized by the effect of natural convection mechanisms, and the radiation heat transfer is neglected since the temperature differences are not high in the system.

Equations 7-11 contain the steps of the method used in the heat convection coefficient calculations used in the model, whose value range is given in Table 2. Heat transfer relations in natural convection are based on experimental studies except for some simple cases. The simple empirical relation for the mean Nusselt number $\overline{Nu}_L$ in natural convection is as follows:

$$\overline{Nu}_L = \frac{h.L}{k} = C \cdot Ra_L^n \tag{7}$$

where h is the heat convection coefficient (W/m^{2}K), L is the length of the geometry (m), k is the heat conductivity (W/m·K), C is a constant coefficient, Ra_L is the Rayleigh number which is the product of Grashoff (Gr_L) and Prandtl (Pr) numbers, and n is a constant exponent. They are given as:

$$Ra_L = Gr_L \cdot Pr = \frac{g \cdot \beta \cdot (T_s - T_\infty) \cdot L^3}{\nu \cdot \alpha} \tag{8}$$

$$Gr_L \equiv \frac{g \cdot \beta \cdot (T_s - T_\infty) \cdot L^3}{\nu^2} \tag{9}$$

where g is the acceleration of gravity (m/s^2), β is the coefficient of volumetric expansion (1/^{o}K) and can be expressed as β=1/T for ideal gases, T_s is the surface temperature (^{o}C), T_∞ is the fluid temperature far enough from the surface (^{o}C), ν is the kinematic viscosity of the fluid (m^2/s) and α is the thermal diffusivity of the fluid (m^2/s).

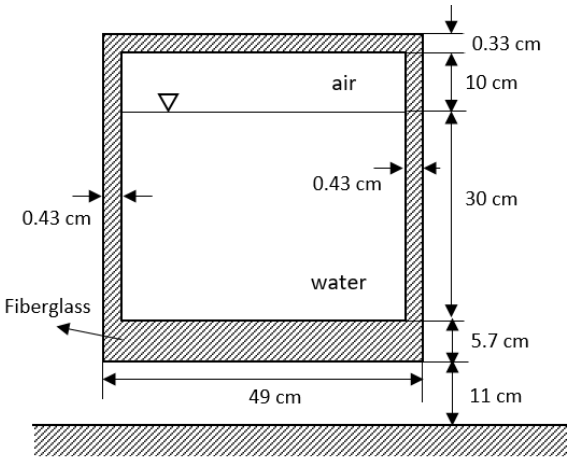

Figure 6. Schematic view of the geometry of the container.

The Nusselt number for the vertical walls can be expressed by the following relation:

$$\overline{Nu}_L = \left\{ 0.825 + \frac{0.387 \cdot Ra_L^{1/6}}{\left[1 + (0.492/Pr)^{9/16}\right]^{8/27}} \right\}^2 \tag{10}$$

For the horizontal top cover or horizontal bottom base, the appropriate one of the following relations is used to determine the Nusselt number:

$$\begin{aligned} \overline{Nu}_L &= 0.54 \cdot Ra_L^{1/4} \quad (10^4 \le Ra_L \le 10^7) \\ \overline{Nu}_L &= 0.15 \cdot Ra_L^{1/3} \quad (10^7 \le Ra_L \le 10^{11}) \\ \overline{Nu}_L &= 0.27 \cdot Ra_L^{1/4} \quad (10^5 \le Ra_L \le 10^{10}) \end{aligned} \tag{11}$$

After the $\overline{Nu}_L$ number was calculated with the help of the relations given above, the heat convection coefficients (h) on the surfaces were calculated using Eq. (7). The range of heat

convection coefficient values calculated by this method is given in Table 2.

In this study, the thermal resistance model is used, and this concept is based on the analogy between electric current and heat dissipation. The relationship between electrical resistance and transmitted electric current is analogues to the relationship between thermal resistance and transmitted heat power. Resistance is defined as the ratio of a potential difference to current while thermal resistance is defined as the ratio of the temperature difference to the heat power transmitted. Equivalent thermal circuits can also be used for complex systems such as mixed walls. When the layers of such walls are composed of different materials, they can contain many series and parallel thermal resistances. The schematic of the thermal resistance circuit of the device in the steady-state for the geometry in the study is shown in Figure7.a. The thermal circuit consists of the side thermal resistances and the thermal capacitances of the fiberglass box, water and the still air, Combining the series and parallel thermal resistances, their equivalent circuit shown in Figure 7.b is obtained.

By adding a thermal capacitance to the equivalent thermal resistor in parallel to model thermal dynamics, the transient thermal circuit model shown in Figure 7.c is obtained. For the device, the side thermal resistance components of the box, the bottom thermal resistance of the box, and the top thermal resistance of the box, are, respectively, given as

$$R_{con-inner} = \frac{1}{h_{inner} A_{side}} \tag{12}$$

$$R_{THwall} = \frac{d_{wall}}{k_{fg} A_{side}} \tag{13}$$

$$R_{con-outer} = \frac{1}{h_{inner} A_{side}} \tag{14}$$

and

$$R_{THdown} = R_{THup} = \frac{d}{k_{fg} A_{down}} \tag{15}$$

where d_{wall} is the thickness of the glass fiber, h_{outer} is the wall-to-air heat convection constant, h_{inner} is the water-to-wall heat convection constant, and k_{fg} is the thermal conductivity of the glass fiber, A_{side} is the side (wall) area which is the vertical surface area (m^2) where heat transfer takes place, and A_{down} is the base or ceiling area.

Since they are four side thermal resistances, and one cover thermal resistance, and one base thermal resistance, their equivalent thermal resistance of the device is given as

$$R_{TH} = (R_{con}/4) // (R_{THdown}/2) \tag{16}$$

$$R_{TH} = \frac{R_{con}\, R_{THdown}}{8\left(\frac{R_{con}}{4} + \frac{R_{THdown}}{2}\right)} \tag{17}$$

where $R_{con} = R_{con-inner} + R_{THwall} + R_{con-outer}$,

The heat power transferred to the environment in the steady-state can be expressed using the thermal resistance method as follows:

$$p = \frac{\Delta T}{R_{TH}} = \frac{(T_w - T_a)}{R_{TH}} \tag{18}$$

where T_w is the water temperature and assumed to be the measured water temperature $T(t)$.

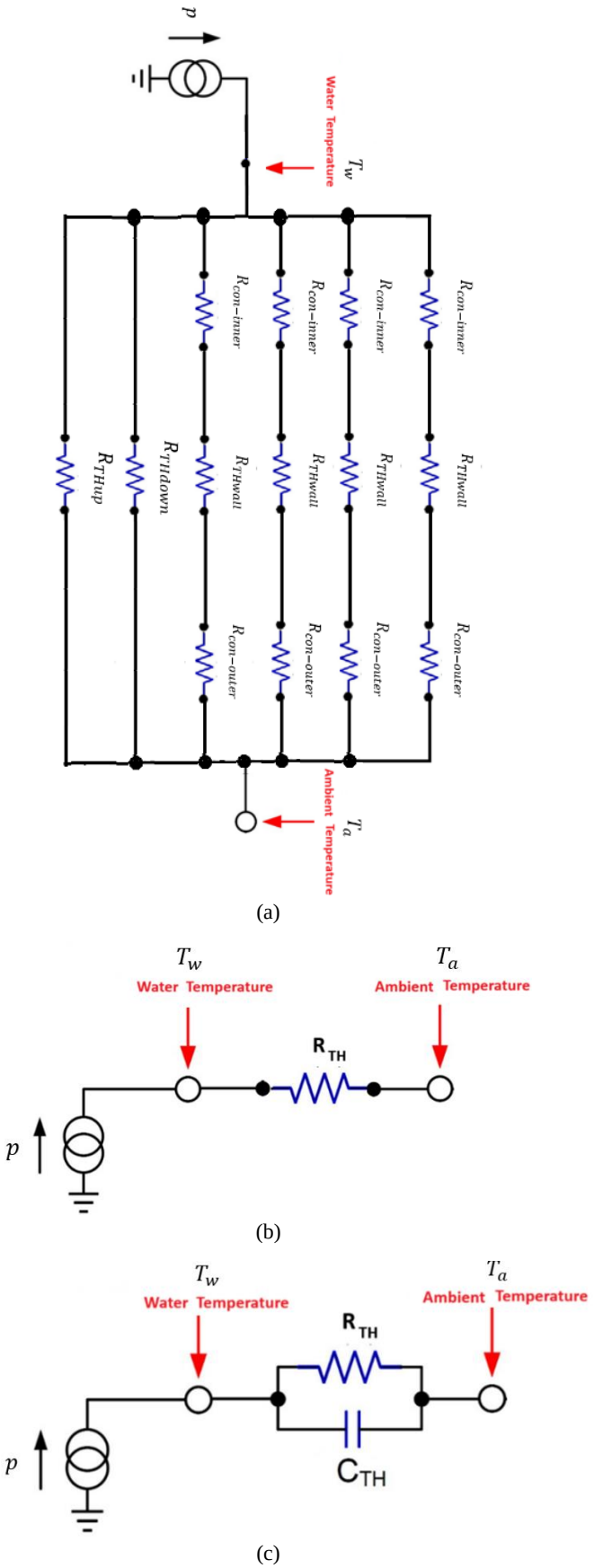

Figure 7. *a) The steady-state thermal circuit of the chamber, b) the steady-state equivalent thermal circuit of the chamber, and c) the transient thermal circuit model of the chamber.*

Heat convection coefficient values were calculated for the outer, inner, top, and bottom surfaces of the container side walls. The equivalent thermal resistance is calculated as 0.0243 W/K with the parameters given in Table 2.

Table 2. The thermal parameters.

Parameter	Symbol	Value
The ambient temperature	T_A [°C]	25
The set water temperature	T_{ref} [°C]	75
Heat convection coefficient	h [W/(m^2·K)]	4.95-5.81
Heat conductivity of fiberglass	k_{fg} [W/(m·K)]	0.040
Heat conductivity of air	k_a [W/(m·K)]	0.026-0,030
Heat conductivity of water	k_w [W/(m·K)]	0.613-0,688
Specific heat of water	C [J/kg°C)]	4186
Kinematic viscosity of air	ν_{air} [m^2/s]	18.45×10^{-6}
Kinematic viscosity of water	ν_w [m^2/s]	6×10^{-7}
Prandtl number for air	Pr_{air}	0.7
Prandtl number for water	Pr_w	4.0

The thermal capacitance of water is found as

$$C = mc \tag{18}$$

where m is the mass of water and c is the specific heat of water.

The mass of water within the chamber is approximately 100 kg, The thermal capacitance of the water (C) or the device ignoring the mass of other sections is calculated to be 418740 J/°C. In the transient, the heat transfer model of the device can be modeled as

$$p = DV_{rms}^2/R_{AC}(T) = mc\frac{d(T_W - T_{A)}}{dt} + \frac{T_W - T_A}{R_{eq}} \tag{19}$$

where T_A the ambient temperature, T_W is the water temperature, m is the water mass, and c is the specific heat of water.

In the steady-state, since the temperature of the device is not varying with time and the water temperature is 75 ^{0}C, the power consumption of the device can be modeled as

$$p = DR_{AC}(T_W)I_{rms}^2 = DV_{rms}^2/R_{AC}(T_W) = \frac{T_W - T_A}{R_{eq}} \tag{20}$$

where I_{rms} is the rms current of the heater resistance and $R_{AC}(T)$ is the temperature dependent heater resistance.

6. Simulation Results

The system simulations are performed in Matlab program. The system is simulated under heating conditions when the full electrical power 2000 W is applied to the device, and the water temperature during the heating process is shown in Figure 8.a. The simulated water temperature is almost a ramp in this case. The system is simulated under natural cooling conditions, and the water temperature during the cooling process is shown in Figure 8.b. The simulated temperature falls exponentially when simulated for 6 hours.

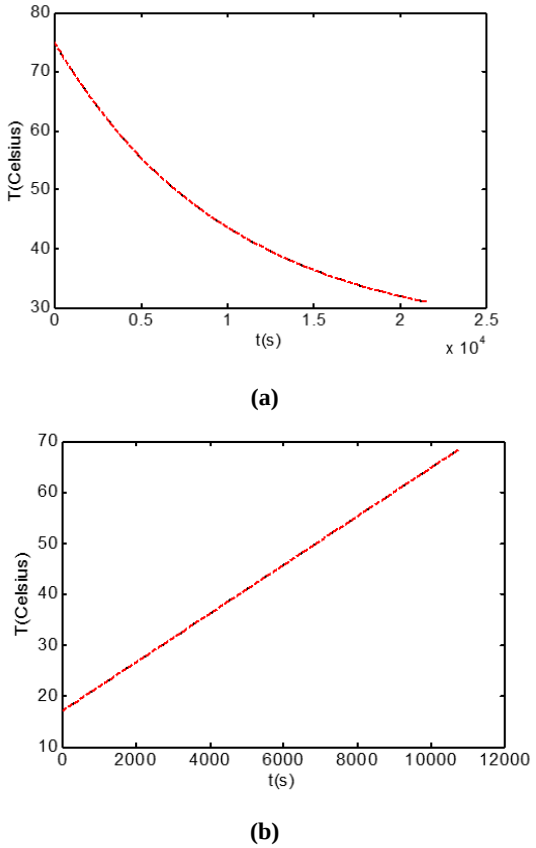

Figure 8. *Simulated temperature vs. time during a) the natural cooling of the device and b) the heating process.*

7. Experimental Results

The water absorption test on a marine power cable is made to ascertain the quantity of water absorbed by the insulation when it comes into contact with water. To be able to use the device in such a test, the device's performance must be examined. In this study, experiments are done to see the performance of the water absorption chamber designed. Before starting the test, the device is filled with tap water. The water chamber is placed in the test room for protection purposes during high voltage experiments. As a result, there is neither forced nor natural cooling of the device during the test. In the test, a 4,5 meter long 0.6 /1 kV Volt rated marine cable after removing the outer TPO sheath and armoring is placed within the chamber as shown in Figure 9 and the device is turned on. Its temperature is read from the controller display shown in Figure 10 and recorded with respect to time. Two thermal experiments were conducted on the device. The first experiment was performed during the heating of the device, and the other during its natural cooling. In the first experiment, the device was turned on at room temperature, and the water temperature was read every few minutes until it reached 75 °C. The heating duration or the setting time of the device can be assumed to be almost 3 hours. After this time, its resistor is turned on and off to compensate for the ambient power loss. The time and temperature data were recorded and plotted. In the second experiment, the water temperature was at 75 °C, and the device

was in the thermal steady-state when it was turned off. As the device cooled, the temperature and time data were also recorded. The graphs showing the temperature as a function of time from these experiments are shown in Figure 11.

Figure 9. *A photograph of the water absorption test from the laboratory*

Figure 10. *The appearance of the device monitor during the experiment in the steady-state.*

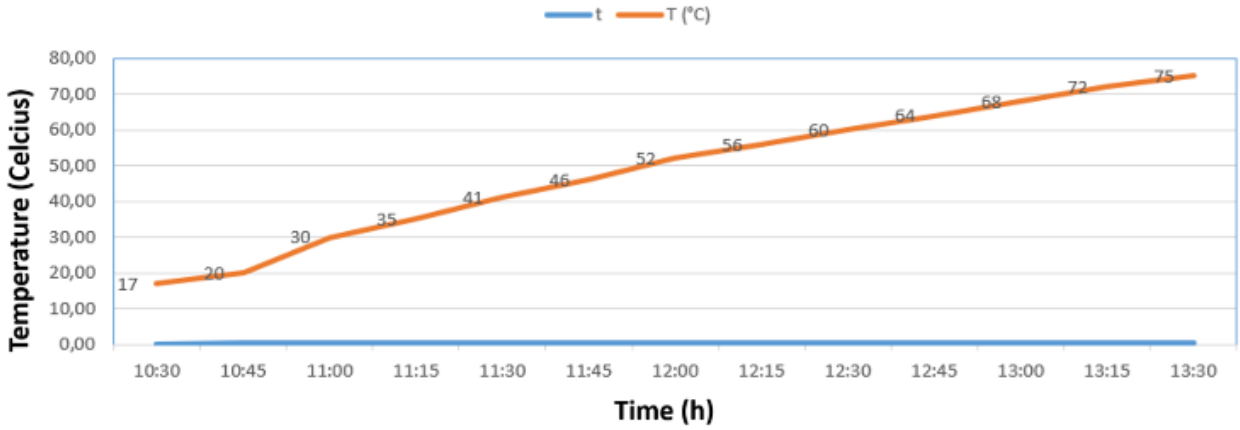

(a)

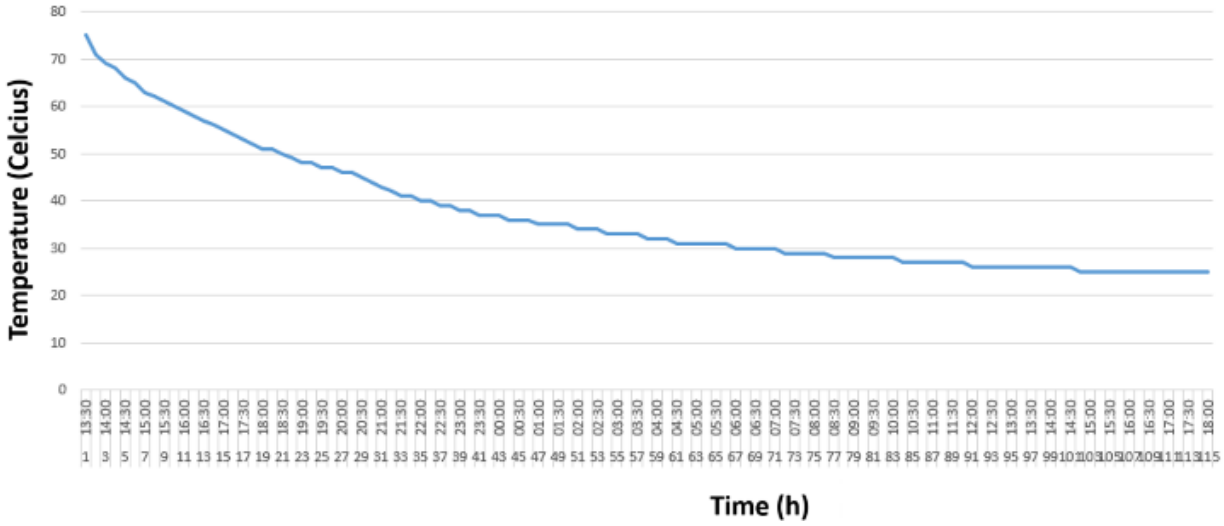

(b)

Figure 11. *Temperature vs. time during a) the heating process and b) the natural cooling of the device.*

The experiment shows that the device performs well. When the utility voltage is 220 Volt, the water temperature reaches from 18 ^{0}C to 75 ^{0}C, i.e., to the thermal steady-state in almost 3 hours. When the device is turned off, the water temperature falls to the ambient temperature in almost 5,5 hours as seen in Figure 11.b. The specific heat capacitance of the model is found to be 4.026e+05 J/°C which gives an acceptable error of just -3.99%. The error of the thermal resistance is found to be much higher than the calculated value. The decay of the temperature is not exponential enough. Therefore, the thermal dynamics are more complex than the behavior of the simplified model. This means the thermal model of the device should be modified. Heat transfer equation can be solved in Cartesian coordinates with proper boundary conditions using finite difference or finite element method to improve the heat transfer model of the circuit. Also, an experiment with multiple temperature sensors can be done to measure the thermal conductivity of the insulator material to check its accuracy. However, the device operates well performing its duty during the tests without any problem.

8. Conclusion

In this study, a water absorption chamber is designed using fiberglass and it is controlled with a cheap industrial controller by sensing its temperature with a thermocouple. It is tested using a power cable inside. It has been found that it operates well and it is usable to make the tests described in IEEE 1580-2021, NEMA WC 53, and NEMA WC 57 standards.

As future work, we suggest using a fuzzy logic controller to reduce the power consumption of the device. Such a system could benefit from user experience and consider ambient temperature and its derivative as additional inputs. This approach can decrease the setting time and provide tighter temperature error control [31]. The system can also be improved by incorporating IoT for monitoring [32]. IoT can make tracking the water temperature easier and can also be used to stop the experiment if something goes wrong with the operation. The proposed device can be easily modified for larger-scale industrial applications. For instance, using a higher power heater can reduce the heating duration. A larger version of this device can be made for medium voltage cables. The heater power should also be increased accordingly in this case. Additionally, the device is already suitable for mass production due to its simplicity and robustness. Such a chamber can also be combined with a high-voltage generator for better control and monitoring of the experiments.

As another future work, the thermal model of the system can be improved with the methods suggested in the experimental results section.

Author Contribution

Formal analysis – Ercan Ulutay (EU), Reşat Mutlu (RM), Uğur Akyol (UA), Metin Yurtsever (MY); Investigation – RM, UA, MY; Experiments – Avşin Öztaş (AÖ), EU; Processing – MY, EU, RM, AÖ; Literature review – RM, AÖ; Writing – MY, EU, RM, UA, AÖ; Review and editing – RM, UA, MY, AÖ, EU.

Declaration of Competing Interest

The authors declared no conflicts of interest with respect to the research, authorship, and/or publication of this article.

Acknowledgements

This study has been supported through the project UPN -2402 funded by the research and development center of Ünika Üniversal Kablo Sanayi ve Tic. A.Ş. The researchers are thankful to Samet Sarı, Fatih Yerişenoglu, and Sedef Özcan for their assistance.

References

[1] Moore, G. F. (Ed.) (1997). Electric cables handbook, Blackwell Science, UK.

[2] Thue, W. A. (Ed.) (2017). Electrical power cable engineering, CRC Press, Boca Raton.

[3] Tan, R. K., Önder, K., Yerişenoğlu, F., & Mutlu, R. (2023). Usage of an Excel spreadsheet for a thermal endurance test report. *European Journal of Engineering and Applied Sciences*, 6(2), 91-97.

[4] Yurtsever M., Öztaş A., & Mutlu, R. (2024). Assessing the relationship between color change and tensile strength in Thermoplastic Polyolefin outer sheaths of low-voltage power cables. *Trakya University Journal of Engineering Sciences*, 25(1), 11-19.

[5] Georgallis, G. (2021). *Submarine cables. The global cable industry: materials, markets, products*, Wiley Online Library.

[6] Worzyk, T., Submarine power cables: design, installation, repair, environmental aspects. Springer Science & Business Media, pp. 291-310. 2009.

[7] Karhan, M., Çakır, M. F., & Uğur, M. (2021). A new approach to the analysis of water treeing using feature extraction of vented type water tree images. *Journal of Electrical Engineering & Technology*, 16, 1241-1252.

[8] Karhan, M., Çakır, M. F., & Uğur, M. (2020). Analysis of electric field and potential distribution of experimental setup for initiating and growing vented type water trees using finite element method. *Journal of Science and Arts*, 20(3), 755-766.

[9] Standard, IEEE. (2021). IEEE 1580-2021. *IEEE Recommended practice for marine cable for use on shipboard and fixed or floating facilities.* IEEE. https://standards.ieee.org/ieee/1580/7228/, (Access date; March 28, 2022).

[10] NEMA WC 53 standard, https://webstore.ansi.org/standards/nema/ansinemawc53icea275812020, (Access date; March 15, 2022).

[11] NEMA WC 57 standard, https://webstore.ansi.org/standards/nema/ansinemawc57icea735322021, (Access date; March 15, 2022).

[12] Badmera, V., & Patel, R. R. (2017). Electrical characterization of XLPE cable using accelerated water absorption test on medium voltage power cable and partial discharge test on power cable with termination defects. In

2017 Innovations in Power and Advanced Computing Technologies (i-PACT) (pp. 1-7). IEEE.

[13] Brain, M., & Elliott, S. A. R. A. (2006). How water heaters work. (Access date; December 26, 2023)

[14] Duff, C. A., Design of a temperature controllable demand water heater, (2012), PhD, University of Johannesburg, Johannesburg, South Africa.

[15] Biddle, R., Wetzel, J. R., & Cech, R. (1997). Design and performance of low-wattage electrical heater probe. In *38th Annual Meeting of the Institute of Nuclear Materials Management* (pp. 20-24). Los Alamos National Lab.

[16] Cheng, C., Lin, J., Zhang, H., Wang, Q., Xi, L., Wang, L., & Luo, C. (2023). Design and research of power battery temperature control by PLC. *Frontiers in Computing and Intelligent Systems*, 4(1), 63-66.

[17] Abdurahman, A., Sunardi, S., Sugeng, S., Setiawan, J., & Syukur, A. M. (2022). Design of PLC based temperature control system for food stability test chamber. *Sebatik*, 26(2), 482-488.

[18] Ghafourian, J., Avashbeigi, S., Hedayatnia, A., & Rezvanijalal, J. (2023). Implementation of PID controller for sequential control of flow, level and temperature in Festo MPS PA compact workstation by PLC. In *7th International Conference on Electrical, Computer and Mechanical Engineering* (pp. 1-10).

[19] Rahmadini, V. F., Ma'arif, A., & Abu, N. S. (2023). Design of water heater temperature control system using PID control. *Control Systems and Optimization Letters*, 1(2), 111-117.

[20] Zhao, J., & Wang, W. (2022). Application and study of kiln temperature control system based on PLC. *Journal of Physics: Conference Series*, 2378(1), p. 012021.

[21] Rahmadini, V. F., Ma'arif A., & Abu, N. S. (2023). Design of water heater temperature control system using PID control. *Control Systems and Optimization Letters*, 1(2), 111-117.

[22] Khairunnas, M. D., Ariyanto, E., & Prabowo, S. (2018). Design and implementation of smart bath water heater using Arduino. In *2018 6th International Conference on Information and Communication Technology (ICoICT)* (pp. 184-188). IEEE.

[23] Harvey, M. E. (1968), Precision temperature-controlled water bath. *Review of Scientific Instruments*, 39(1), 13-18.

[24] Chakraborty, S., Bera, S. K., Bera, S. C., & Mandal, N. (2018). Design of a simple temperature transmitter circuit of an electric heater operated water bath. *IEEE Sensors Journal*, 18(8), 3140-3151.

[25] Rashidmardani, A., & Hamzei, M. (2013). Effect of various parameters on indirect fired water bath heaters' efficiency to reduce energy losses. *International Journal of Science and Engineering Investigations*, 2(12), 17-25.

[26] Liang, Z., Zheng, Y., Zhou, N., & Liu, S. (2019). User research–based design strategy for an electric water heater and its application. *IOP Conference Series: Materials Science and Engineering*, 573(1), p. 012052.

[27] Shabanian, S., Ashrafizadeh, F., Saeidi, N., & Ashrafi, A. (2016). Failure analysis of carbon steel components in a water bath heater and the influence of ethylene glycol concentration. *Engineering Failure Analysis*, 66, 533-543.

[28] Tinianov, B., Nakagawa, M., & Muñoz, D. (2005). Prediction of the thermal conductivity of fiberglass insulation using propagation constant: A technique overview. *The Journal of the Acoustical Society of America*, 117(4_Supplement), 2555-2555.

[29] https://enda.com/automation/temperature-controllers/et4420/etx420.pdf, (Access date; December 26, 2024)

[30] Salmaz, E., Kaplan, B., Akkuş, G., Zorlu, S., & Özdaş, D. Ö. (2023). Farklı ışık kaynakları polimerizasyonda ne kadar ısı oluşturur?. *Selcuk Dental Journal*, 10(4), 300-305.

[31] Juang, C. F., & Chen, J. S. (2006). Water bath temperature control by a recurrent fuzzy controller and its FPGA implementation. *IEEE Transactions on Industrial Electronics*, 53(3), 941-949.

[32] Yener, T., Yener, Ş. Ç., & Mutlu, R. (2019). An IoT-based PDCS system. In *International Informatics and Software Engineering Conference (UBMYK)*, (pp. 1-4). IEEE.